

Vibration-induced climbing of drops

P. Brunet,* J. Eggers, and R.D. Deegan
*Department of Mathematics, University of Bristol,
 University Walk BS8 1TW Bristol, United Kingdom.*
 (Dated: October 27, 2018)

We report an experimental study of liquid drops moving against gravity, when placed on a vertically vibrating inclined plate, which is partially wet by the drop. Frequency of vibrations ranges from 30 to 200 Hz, and above a threshold in vibration acceleration, drops experience an upward motion. We attribute this surprising motion to the deformations of the drop, as a consequence of an up/down symmetry-breaking induced by the presence of the substrate. We relate the direction of motion to contact angle measurements. This phenomenon can be used to move a drop along an arbitrary path in a plane, without special surface treatments or localized forcing.

PACS numbers:

A drop of liquid on an inclined substrate will slide downward due to gravity, unless the drop is pinned by contact angle hysteresis [1, 2]. Since the contact angle hysteresis is reduced by vertical vibrations [3, 4], one might expect that sufficiently strong shaking will always make the drop come loose and provoke it to slide. Here we report for the first time that on the contrary, sufficiently strong harmonic shaking in the vertical direction will always cause the drop to climb up the slope, regardless of system parameters.

We attribute the upward force to a combination of the broken symmetry caused by the inclination of the substrate with respect to the applied acceleration and the nonlinear frictional force between the drop and the substrate. During the downward acceleration phase, the drop becomes taller and thus more compliant to lateral forcing. Hence, the maximum value of the contact angle attained on the upper side (Fig. 1(d)) is greater than the maximum value attained on the lower side (Fig. 1(b)), and the drop thus experiences a net upward force [5]. However, for a purely linear frictional force the net force on the drop would average to zero over one period; hence some nonlinearity in the interaction between the drop and the substrate is needed. This key issue is illustrated by a model calculation below.

In our experiments a drop of a glycerol-water mixture, of volume V between 0.5 and 20 μl was deposited on a plexiglass substrate inclined to the horizontal with an angle α up to 85° . The resulting sessile drop was between 1 and 3 mm in diameter, and pinned in the absence of shaking. The substrate was oscillated vertically using an electromagnetic shaker with acceleration up to $50g$ where g is the acceleration due to gravity, and frequencies between 30 Hz and 200 Hz. The acceleration was monitored with a single-axis accelerometer; the acceleration due to unwanted lateral motion did not exceed 3% of the vertical acceleration.

The kinematic viscosity ν of the various mixtures

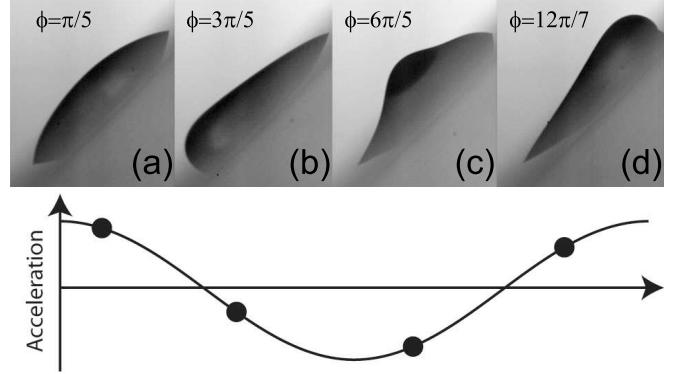


FIG. 1: Side view of a climbing drop (and its reflection) on a vibrating plate inclined at $\alpha=45^\circ$ at different phases ϕ of the cycle. Images (b) & (d) show the maximum lower and upper contact angle, respectively. Parameters are $V=5 \mu\text{l}$, $f=60 \text{ Hz}$ ($f/f_0=1.18$), $a/a_0 = 1.03$, $\nu = 31 \text{ mm}^2/\text{s}$. The lower plot shows acceleration versus phase and the corresponding acceleration for each of the images.

ranged between 31 and 55 mm^2/s . For lower viscosities the drop can break up before the onset of climbing; for higher viscosities, drops move slower and thus their dynamics is more difficult to access. The surface tension γ was equal to 0.066 N/m, the density ρ at 20°C ranged from 1190 kg/m^3 for $\nu = 31 \text{ mm}^2/\text{s}$ to 1210 kg/m^3 for $\nu = 55 \text{ mm}^2/\text{s}$. The contact line angle and position were measured visually using a high speed camera and diffuse back-lighting. The advancing and receding contact angles were measured to be $\theta_a = 77 \pm 2^\circ$ and $\theta_r = 44 \pm 3^\circ$ by inflating or deflating a drop with a syringe and observing the yielding point of the contact line.

The acceleration $a = (2\pi f)^2 A$, where A and f are the amplitude and frequency of the applied vibrations, induces a rocking motion of the drop as shown in Fig. 1. When the rocking motion is large enough, the contact line begins to unpin. The resulting mean motion of the drop depends on the values of a and f as shown in Fig. 2. The drop can move down the substrate (sliding), remain stationary (static) or move up the substrate (climbing).

*Electronic address: p.brunet@bristol.ac.uk

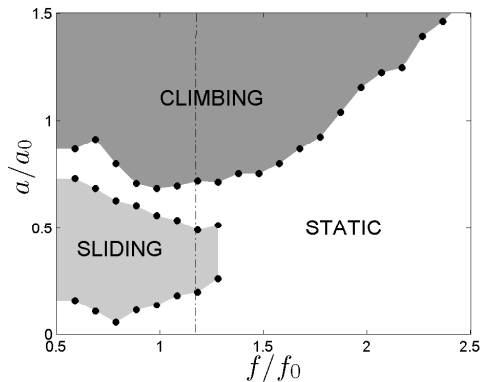


FIG. 2: Phase diagram of drop motion for $V=5 \mu\text{l}$, $\alpha=45^\circ$, and $\nu=31 \text{ mm}^2/\text{s}$. The normalization factors are $f_0 = 50.77 \text{ Hz}$ and $a_0=174 \text{ m/s}^2$.

We obtained similar phase diagrams for different drop volumes, viscosities, and angles of inclination α . While the boundaries of each regime shift as these parameters are varied, the qualitative appearance of the diagram remains unchanged. All results reported below are for the parameters of Fig. 2. As units of frequency and length, we choose the resonance frequency of the drop's rocking mode $f_0 = 50.77 \text{ Hz}$ and the linear drop size $V^{1/3} = 1.71 \text{ mm}$, as this is a measure of the deformation. The value of the former is calculated from the expression given in [6] (eq. (6)), with $\theta_e = 62^\circ$ as calculated from $\cos \theta_e = (\cos \theta_a + \cos \theta_r)/2$ and the geometrical parameter $h=1$; our value is similar to that measured by [7, 8]. We take $a_0 = (2\pi f_0)^2 V^{1/3} = 174 \text{ m/s}^2$ as the characteristic acceleration.

The drop speed U in terms of the capillary number $\text{Ca} = \rho\nu U/\gamma$ versus the normalized acceleration for fixed frequency $f/f_0=1.18$ is plotted in Fig. 3(a). $\text{Ca} = 10^{-3}$ corresponds to a speed of 1.79 mm/s . The data shows that as the acceleration is raised the motion transitions from static to sliding, back to static, and finally to climbing. In the sliding phase, speeds are two orders of magnitude smaller than typical climbing speeds, as shown in the inset. For other parameters (e.g. $V=10 \mu\text{l}$, $f=60\text{Hz}$ or $V=5 \mu\text{l}$, $f=45 \text{ Hz}$) the capillary number threshold for climbing remains the same, but the threshold for sliding varies significantly.

Based on our high-speed observation of the drop viewed from above, we interpret the progression through the stuck, sliding, and climbing regimes as follows. For low accelerations the contact line is pinned at all point on the perimeter. As the acceleration increases the pinning progressively breaks due to the rocking motion until a few points on the side of the drop remain pinned, and only temporarily (see Fig. 4(1) showing sliding). As the acceleration continues to increase, the upward force due to shaking cancels out gravity, to produce an almost vanishing net force. At this point the drop repins along its sides, and becomes stationary again (see Fig. 4(2)). Yet

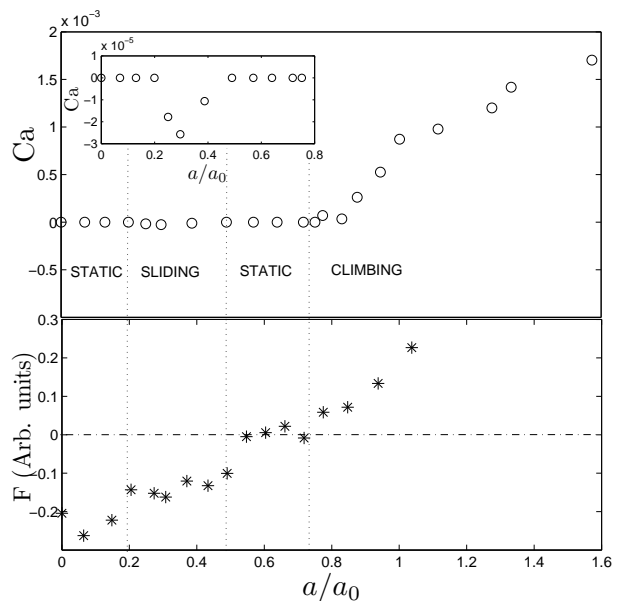


FIG. 3: *Top* - The capillary number Ca vs. a/a_0 ($f=60 \text{ Hz}$, $V=5 \mu\text{l}$, $\nu=31 \text{ mm}^2/\text{s}$), measured along the dot-dashed line in Fig.2. Inset: magnified view of data below the climbing threshold. $\text{Ca} = 10^{-3}$ corresponds to a speed of 1.79 mm/s . *Bottom* - Estimate of the force averaged over a cycle due to the difference between the upper and the lower contact angles.

greater acceleration increases the upward force past the pinning threshold and the drop moves up the substrate (see Fig. 4(3)-(5)).

To support the crucial observation that shaking always produces an upward force, we performed additional experiments using a horizontal plate subjected to an acceleration angled away from the vertical, thus eliminating gravity. The results are depicted in Fig. 5: sessile drops move to the right and pendant drops move to the left. This corresponds to there being nothing but climbing motion in the original inclined plate geometry.

While the drop's contour does not vary significantly over one period, the contour shape is strongly dependent on the drop's global velocity. As shown in Fig. 4, the shape for sliding and climbing drops are similar, but the downslope end tends to sharpen with increasing Ca . Above $\text{Ca} \approx 1.8 \times 10^{-3}$ the trailing end of the drop undergoes a pearling instability similar to the observations of [9, 10] for a drop sliding at constant speed down an incline.

Figure 6 shows the relationship between the instantaneous measurements of the contact line's speed and angle for our drops. The leftmost panel shows an example of raw data for the contact line position at the upper and lower end for a climbing drop: oscillations are superimposed on a slow upward motion. The instantaneous speed was extracted from the position data by subtracting the mean motion, averaging the result over multiple periods to reduce noise and fitting it with a spline, and differentiating the spline. In Fig. 6 the center panel is for a

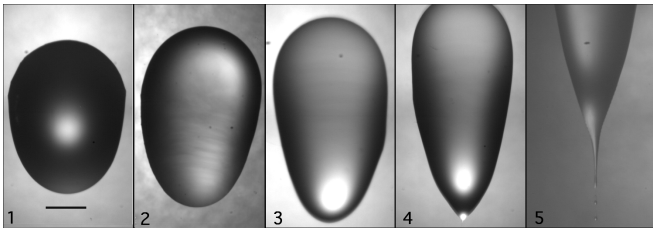


FIG. 4: Views from above of sliding (1), static (2), and climbing drops (3-5). As the speed of the drop increases from (3) to (5), the trailing end transitions to a corner (4), and then to pearling. $a/a_0=0.46$ (1), 0.67 (2), 0.96 (3), 1.13 (4), 1.39 (5). The scale bar equals 1 mm.

sliding drop and the right panel is for a climbing drop.

There is a clear correlation between the instantaneous contact angle and the contact line speed: the maximum speed of the upper and lower contact line coincides with the maximum upper and lower contact angle, respectively. Furthermore, the contact angle is a good indicator of the qualitative difference in the oscillations of a sliding and climbing drop. For a climbing drop the average of the upper contact angle θ_u is larger than the average of the lower contact angle θ_d . In contrast, for a sliding drop the average value of θ_d for a sliding drop is significantly greater than that of θ_u . The uphill shift in the asymmetry of the oscillations with greater acceleration correlates well with the average motion.

Nonetheless, we find no local and instantaneous law relating the contact line speed to the angle. In particular, as indicated by the lack of pinning when the contact angle lies between the advancing and receding contact angle (denoted by the dotted and dot-dashed lines in Fig. 6), the Cox-Voinov law [11, 12] generalized to account for contact angle hysteresis found for steady drop motion [9] does not work. To account for the related phenomenon of drop motion induced by *asymmetric* shaking, Daniel *et al* [7] propose a ratcheting mechanism. This mechanism depends crucially on the drop pinning when the contact angle lies between the advancing and receding contact angles. However, the absence of pinning observed for our system at elevated accelerations, consistent with the observations of [3] and [4], contradicts this explanation.

We obtain a simple contact angle criterion for climbing or sliding from an estimate of the force on the drop, resulting from both the upward driving force and gravity. The unbalanced Young force per unit length of the contact line is $\gamma(\cos\theta - \cos\theta_e)$ [2]. Disregarding variations along the perimeter, the force averaged over a period is [13]

$$F = \frac{1}{T} \int_0^T (\cos\theta_d - \cos\theta_u) dt. \quad (1)$$

The resulting values for the force versus acceleration are plotted in the bottom graph of Fig. 3. A positive value corresponds to a force directed upwards. The force

can be converted to dimensional units by multiplying by $V^{1/3}\gamma = 1.13 \times 10^{-4}$ N. The force becomes positive close to the acceleration threshold for climbing. Below the climbing threshold this force is an inadequate measure of the speed, due to our neglect of the retention forces responsible for contact angle hysteresis. This neglect is only permissible for large accelerations, for which the hysteresis vanishes [3, 4]. Preliminary experiments performed with much smaller hysteresis (drops of silicone oil on a partially wetting fluorinated-coating substrate) show much greater sliding speeds, in accordance with this argument.

The role of a nonlinear friction law between drop and substrate is examined through a simple mechanical model which captures the essence of the drop system. The drop is represented by a straight rod, held upright by a non-harmonic spring, which represents surface tension forces (see Fig. 7). Thus a positive angle ϕ corresponds to the drop rocking forward. The lower end of the rod, whose position is $x(t)$, slides on a one-dimensional rail, which is shaken at an angle α with amplitude A . For fixed $x(t)$, ϕ averaged over one period is nonzero, illustrating the symmetry breaking. We allow for a frictional force $-F_0\dot{x}^\beta$ between the rod and its support. Numerical simulations show net motion only if the frictional force is nonlinear, i.e. $\beta \neq 1$. For $\beta = 1$ the force integrated over one period vanishes, regardless of the dynamics of the drop itself. For $\beta > 1$, the rod generically moves to a given direction which reverses if α changes sign. The net motion arises from a finite α that introduces an asymmetry in the motion $x(t)$ of the rod's base. Thus, over one period the average force $\bar{F} = -F_0/T \int_0^T \dot{x}^\beta dt$ is nonzero, causing the 'drop' to move. To summarize the implications of the model, the only necessary—but crucial—ingredients for droplet motion are a front-aft symmetry breaking, and a non-linear friction law between the drop and the plate.

There are two candidate mechanisms to achieve the latter. First, even though the fluid is Newtonian, the area of contact between the fluid and the plate is changing in time, which makes the relationship between the mean drop speed and the total force non-linear. Second, contact angle hysteresis introduces non-linearity into the force-speed relationship even for a constant drop shape. Preliminary comparisons of the above results with those of smaller hysteresis show that climbing speeds at the same accelerations are comparable. This casts doubt on the necessity of hysteresis for climbing.

We have shown that sessile drops subjected to off-

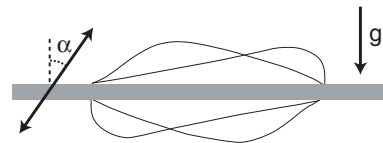


FIG. 5: Drops resting on a horizontal plate (or hanging below it), but shaken at an angle. The drop moves in the direction of the shake pointing normal toward the drop.

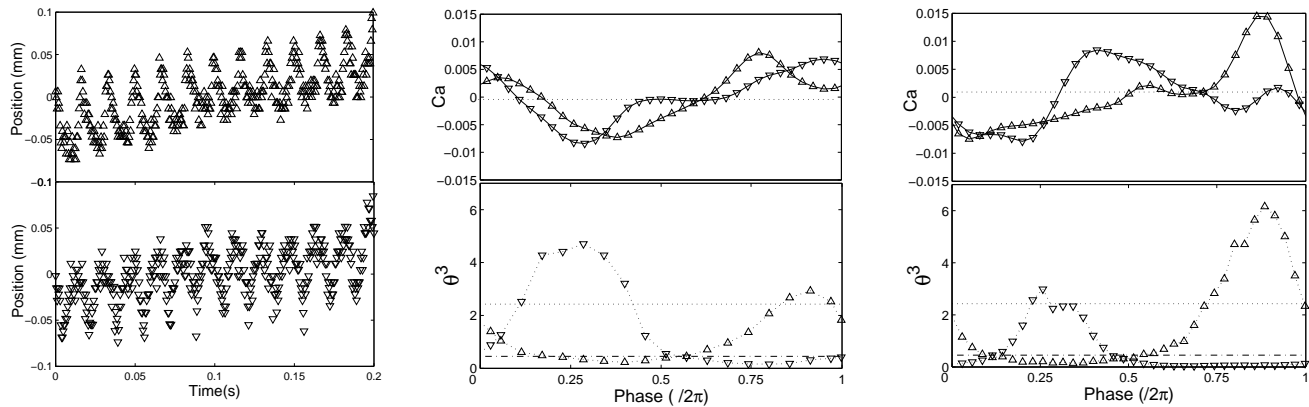


FIG. 6: *Left Panel* - Displacement of the upper (Δ) and lower (∇) contact lines for a climbing drop during 12 periods ($a/a_0=1.03$). *Top Center & Right* - Capillary number versus time for one period of oscillation for a sliding drop (*Center*) and a climbing drop (*Right*). The average Capillary number is denoted by a dotted line dashed line in the *Top* plots. θ_a^3 and θ_r^3 are denoted by dotted and dot-dashed lines, respectively, in the *Bottom* plots. $f=60\text{Hz}$, $V=5\ \mu\text{l}$, $a/a_0=0.45$ (*Center*) and 1.03 (*Right*).

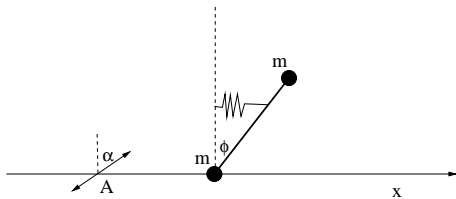


FIG. 7: A mechanical model for moving drops. The support is vibrated at an angle α relative to the vertical. In equilibrium, surface tension holds the drop in a symmetric position, $\phi = 0$. In the horizontal direction, a nonlinear frictional force $-F_0\dot{x}^\beta$ acts between the base of the drop and the support.

vertical vibrations experience a net force tangent to the plate in the direction of the vibrations. Forces greater than gravity can be easily achieved. The manipulation

of sessile droplets is of increasing importance owing to the advent of microfluidics and the need to move fluid packets around microfluidic devices. Our results suggest a device in which droplets can be moved arbitrarily and in parallel by independently varying the phase and amplitude of the vertical and horizontal vibrations for each axis. Recent studies have demonstrated spontaneous drop motion due to gravity fields [10], wettability gradients [14], an interplay between thermal effects and ratcheting [15], asymmetric vibrations [7], and chemisorption [16]. By contrast, our transport mechanism would work for uniform substrates, zero mean forcing, and in the absence of external imposed gradients.

Acknowledgments - We are indebted to J.S. Snoeijer for useful ideas and stimulating discussions. We thank H.A. Stone for fruitful discussions.

-
- [1] E. B. Dussan V. and R. T.-P. Chow, *J. Fluid Mech.* **137** 1 (1983).
 - [2] P.G. de Gennes, *Rev. Mod. Phys.* **57**, 827-863 (1985).
 - [3] C. Andrieu, C. Sykes and F. Brochard, *Langmuir* **10** 2077-2080 (1994).
 - [4] E.L. Decker and S. Garoff, *Langmuir* **12**, 2100-2110 (1996).
 - [5] In experiments, the contact angle lags the acceleration by $\phi/2\pi \approx 0.1$ which explains the appearance of the maximum of the upper contact angle in the upward acceleration phase, and the maximum of the lower contact angle in the downward phase.
 - [6] F. Celestini and R. Kofman, *Phys. Rev. E* **73**, 041602 (2006).
 - [7] S. Daniel, M.K. Chaudhury and P.G. de Gennes, *Langmuir* **21** 4240-4248 (2005).
 - [8] L. Dong, A. Chaudhury and M.K. Chaudhury, *Eur. Phys. J. E* **21**, 231-242 (2007).
 - [9] N. Le Grand, A. Daerr and L. Limat, *J. Fluid Mech.* **541**, 293-315 (2005).
 - [10] T. Podgorski, J.-M. Flesselles and L. Limat, *Phys. Rev. Lett.* **87**, 036102 (2001).
 - [11] R.G. Cox, *J. Fluid Mech.* **168** 169-194 (1986)
 - [12] O.V. Voinov, *Fluid Dyn.* **11**, 714-721 (1976).
 - [13] Although (1) is formally similar to the corresponding force introduced in [7], it differs crucially in that there is no account of hysteresis.
 - [14] U. Thiele and E. Knobloch, *Phys. Rev. Lett.* **97**, 204501 (2006).
 - [15] H. Linke *et al.*, *Phys. Rev. Lett.* **96**, 154502 (2006).
 - [16] Y. Sumino *et al.*, *Phys. Rev. Lett.* **94**, 068301 (2005).